

Characteristic Mode Analysis and Design of Broadband Circularly Polarized CPW-Fed Compact Printed Square Slot Antenna

Jaiverdhan^{1, *}, Mahendra M. Sharma¹, Rajendra P. Yadav¹, and Reshmi Dhara²

Abstract—A CPW-fed printed square slot antenna (PSSA) based on characteristic modes (CMs) theory is investigated for broadband circular polarization (CP). It consists of an I-shaped patch and CPW ground plane loaded with a rectangular stub, a pair of asymmetric inverted-L grounded strips, and a spiral slot to get CP radiation over a wide-angle range. CMs of this strip and slot loaded PSSA show that the entire structure takes participation to excite magnetic and electric modes to provide broadband performance. First six characteristic modes are excited using CPW feeding to find resonating frequencies and radiating behavior. The proposed antenna is fabricated over RO-3003 substrate material with a floor area of $20 \times 20 \text{ mm}^2$. Experimental results showcase the broadband CP performance with wide 3-dB ARBW of 56% (6.6–11.8 GHz) and impedance bandwidth (IBW) ($|S_{11}| \leq -10 \text{ dB}$) about 115% (4–11 GHz) which make it suitable for C-band and X-band wireless and satellite communication applications. The antenna has a peak gain about 5.5 dBi with good LHCP radiations in the broadside direction.

1. INTRODUCTION

With the rapid development in wireless, mobile, and satellite communication technologies, the demand for multiband or dual-band or broadband circularly polarized antennas for ultra-wideband (UWB) applications has been increased. Circular polarization is a well-known characteristic to mitigate the problem of linear polarization (LP) such as Faraday rotation, multipath loss, and polarization loss by avoiding polarization alignment between transmitter and receiver [1]. Printed square slot antennas (PSSAs) have become very popular due to their inherent characteristics of wide impedance bandwidth, compact size, light weight, and easy integration with other devices. PSS antenna has received increasing attention in designs where higher CP bandwidth is desired. Bandwidth is a necessary parameter which can be used to enhance channel capacity and improve high data rate for wireless communication system. In view of above perspective, the need of broadband CP antenna with wide IBW is inevitable. A compact microstrip patch antenna has narrow IBW and ARBW because of its high Q -factor [2]. This shortcoming can enhance the importance of PSSAs. However, in recent years numerous CP techniques have been reported in the literature such as single/dual-feed, fractal structure, and loading of different shapes of strips/slots/stubs on radiating patch and/or ground plane to achieve CP by creating perturbation in electric field which excites two field components of equal magnitude and phase quadrature. Different techniques have been reported in the literature to produce wideband [3–5]/multiband [6, 7]/broadband [8–20] circular polarization characteristics.

However, the CMA analysis is lacking in previously reported literature for the wideband/UWB antennas. In this regard, the proposed strip and slot loaded CP antenna also employs the analysis of CMA for the broadband response. The theory of characteristic mode analysis (CMA) is a fundamental

Received 12 May 2020, Accepted 23 June 2020, Scheduled 13 July 2020

* Corresponding author: Jaiverdhan (2016rec9051@mnit.ac.in).

¹ Department of Electronics & Communication Engineering, Malaviya National Institute of Technology, Jaipur 302017, India.

² Department of Electronics and communication Engineering, National institute of technology Sikkim, India

approach to design and find the resonance of any antennas in free space by computing the surface current and the field radiated by the conducting structure. Firstly, CMA analysis was proposed by Garbacz [21] in 1965 for the wire antenna, and Harrington and Mautz [22] further extended this method for the solid conducting structure. Theory of CMA analysis is based on MoM (Method of Moments) based full wave analysis of electric field integral equations and computes the antenna performance in terms of eigenvalues [23]. In reported literature, a variety of structures has been designed for various purposes like slot, MIMO, metamaterial based, multiband, wideband, and UWB antennas using the theory of characteristic mode (CMA) [24–30]. In this work, CMA analysis is performed using CST MWS simulator in multilayer solver approach. The fundamental need for multilayer solver is that the conductor and dielectric substrate must be loss free, and we set PEC for the patch and ground plane. Characteristic mode denotes the normalized surface current magnitude which depends upon the structure and size of conducting elements.

This work aims to propose a compact, simply structured, broadband CP slot antenna for C-band and X-band applications by applying the theory of characteristic modes. The IBW can be enhanced by exciting first six characteristic modes. To confirm the compactness, simplicity, and CP behavior, a pair of asymmetric inverted-L grounded strips, a spiral slot, and a rectangular stub are embedded on a CPW-fed I-shaped square slot antenna. A prototype of the proposed antenna is also fabricated and experimentally characterized. The proposed antenna is authenticated from a good agreement between the simulated and measured results in detail.

2. THEORY OF CHARACTERISTICS MODES

Characteristic mode can be defined as the orthogonal current modes that are supported on conducting surfaces. CMA is a mathematical approach to calculate a set of current modes of any conducting structure in free space without using feed port. It provides the response in terms of eigenvalues, characteristic angle, surface current, field radiation, and model significance to find dominant resonating modes. It also provides information about different resonances and modes of a wideband or multiband antenna. The electric current over the surface of any conducting body is the summation of CM current or eigen current of the n th mode (J_n) with characteristic angle (α_n).

$$\vec{J} = \sum_n J_n \alpha_n \quad (1)$$

The ratio of reactive power to radiative power provides eigenvalues, and it is used to analyze the CMA and antenna radiation information. Only the lower eigenvalues (λ_n) play a significant role in the antenna radiation, whereas the higher order modes, i.e., larger value of λ_n , do not play a significant role in antenna radiation. To compute the characteristic modes of a conducting surface, the following eigenvalue equation is used.

$$X(J_n) = \lambda_n R(J_n) \quad (2)$$

The impedance matrix is given by $Z = R + jX$, and λ_n is the eigenvalue of the n th characteristics mode. Sometimes, eigenvalue versus frequency plot takes very high values of λ_n , then it is not possible to classify the dominant mode of antenna radiation using eigenvalues. This problem can be mitigated by evaluating new characteristic parameter called model significance (MS) and characteristic angle (α_n), which evaluate all aspects of radiation capability of individual modes. The model significance is computed by using eigenvalues (λ_n) and given by the following equations.

$$\text{MS}_n = \left| \frac{1}{1 + j\lambda_n} \right| \quad (3)$$

Generally, MS has values of one “1” at the resonance point and zero “0” for the modes which do not contribute to the resonance. Modes with small eigenvalues, i.e., $\lambda_n = 0$ are good radiating modes and provide $\text{MS} = 1$. Characteristic angle (α_n) provides the phase difference between J_n and electric field E_n and can be computed from eigenvalues using the following equation

$$\alpha_n = 180^\circ - \tan^{-1}(\lambda_n) \quad (4)$$

Characteristic angle (α_n) has 180° phase difference for the resonating mode, i.e., $\lambda_n = 0$, where it radiates; otherwise, energy is stored which is indicated by characteristic angles having values 90° or 270° .

2.1. Characteristic Mode Performance Analysis

In this section, the CMA performance of proposed strip and slot loaded broadband circularly polarized antenna is explored. Fig. 1 depicted the proposed antenna structure and plot of eigenvalues versus frequency plot of the six fundamental characteristic modes. For the effective antenna radiation, the eigenvalue should be zero ($\lambda_n = 0$). Our aim is to achieve a wideband performance of the proposed antenna that can be achieved by exciting multiple modes simultaneously. It is observed that eigenvalues of mode 1, mode 3, mode 4, mode 5, and mode 6 contribute dominant radiation at their respective frequencies in the form of strong EM radiation while mode-2 provides weak radiation because it has very high eigenvalues ($\lambda_n > 0$). This mode (mode 2) is called inductive mode because of its high eigenvalues. These characteristic modes simultaneously provide resonances at 4.4 GHz, 6 GHz, 8.8 GHz, 10 GHz, and 12 GHz, respectively. From eigenvalues, it is found that it may allow an understanding of EM properties of the antenna without considering the input power and surface current. Fig. 2 depicts the plot of model significance and characteristic angles with respect to frequency for the first six characteristic modes. It is observed from Fig. 2(a) that mode 1 shows large model significance value around 1 at the first resonant frequency 4.4 GHz. Mode 2 is non-resonant mode because of very small value of model significance (< 0.2). Similarly, other higher-order modes, i.e., mode 3, mode 4, mode 5, and mode 6, provide large model significance value around 1 at 6 GHz, 8.8 GHz, 10 GHz, and 12 GHz, respectively. Moreover, the characteristic angle signifies that antenna resonates at 180° . It stores magnetic energy (inductive) when it is less than 180° , and it store electric charge (capacitive), when it is more than 180° . From Fig. 2(b), mode 1 crosses 180° axis line at resonant frequency 4.4 GHz, which remains dominant mode, and mode 3, mode 4, mode 5, and mode 6 cross at 6 GHz, 8.8 GHz, 10 GHz, and 12 GHz, respectively [see Fig. 2]. Mode 2, non-resonant mode, has not crossed the 180°

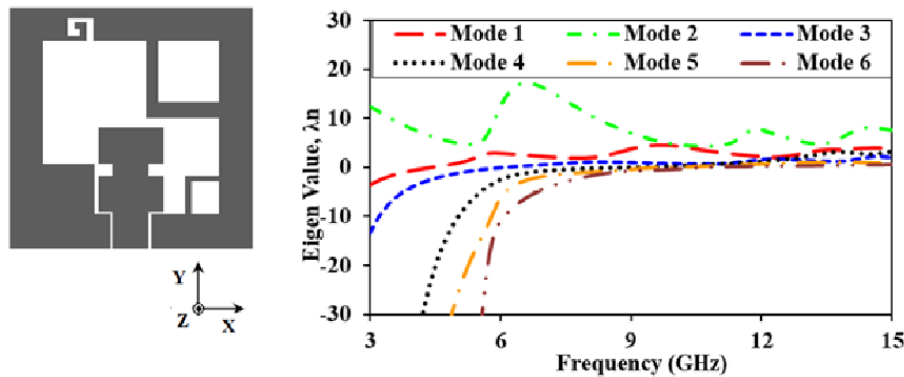


Figure 1. Antenna geometry and eigenvalues versus frequency plot of proposed antenna.

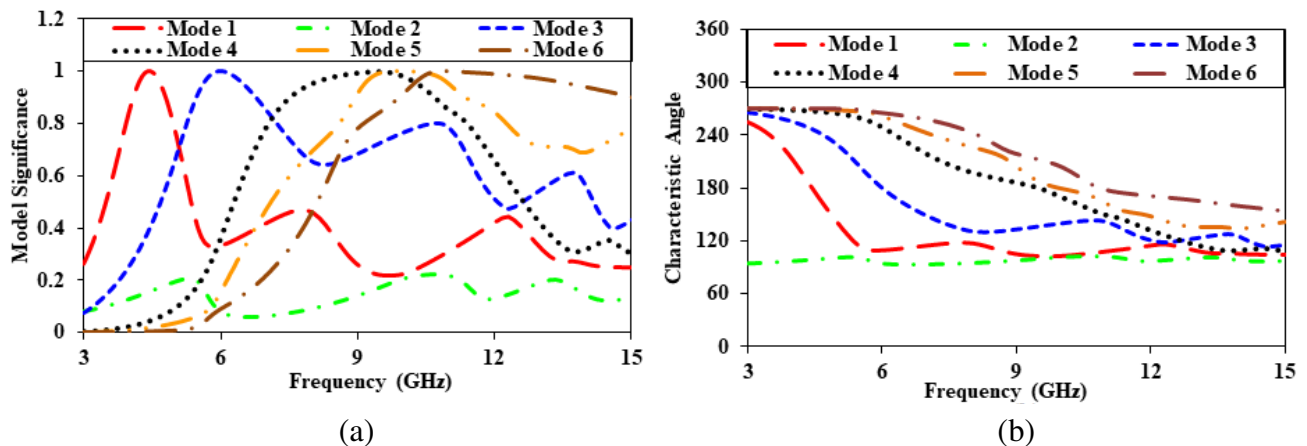


Figure 2. (a) Model significance, (b) characteristic angle plot of the first six CM modes.

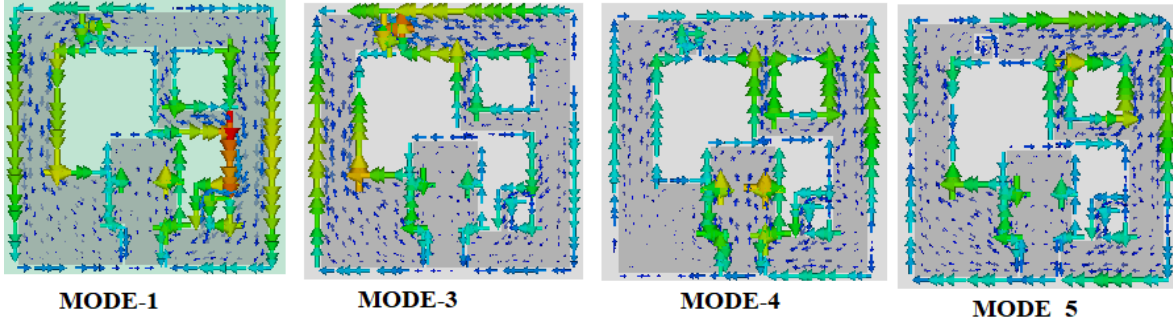


Figure 3. Model surface current of proposed antenna at resonant CMs frequencies.

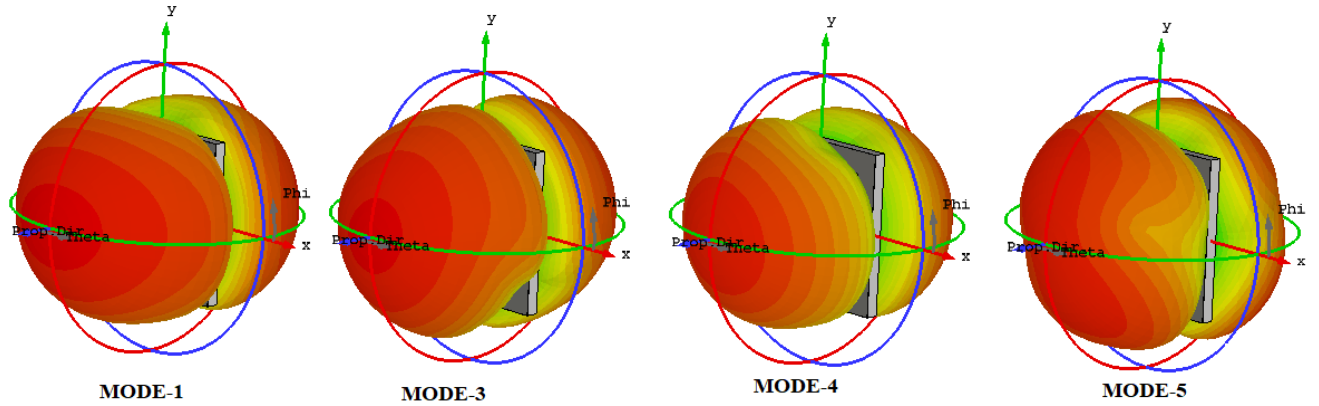


Figure 4. Model 3-D radiation pattern at resonant CMs frequencies.

axis line.

The model surface currents around the resonant frequencies of proposed antenna at excited modes, i.e., mode 1, mode 3, mode 4, and mode 5, without feed port are shown in Fig. 3. The surface current distribution over the radiating element and ground plane generates either odd mode or even mode. With the Galerkin's matching [31], the Method of Moments matrix becomes complex whose eigenspace is a combination of consecutive pair of odd and even modes. This simultaneous excitation of such modes (i.e., even and odd modes) provides the wideband radiation behaviour of an antenna. Fig. 4 shows the 3-D radiation pattern at different characteristic modes with their respective resonant frequency. It is observed from the radiation pattern that all CMs provide main lobe radiation (maximum field) along the xy -plane and null radiation along the y -axis. This concludes that all CMs generate omnidirectional radiation patterns on their respective resonant frequencies.

3. ANTENNA DESIGN AND ANALYSIS

3.1. Antenna Geometry

Figure 5 depicts the geometry layout of the proposed CPW-fed printed square slot antenna for wideband circular polarization. The antenna is designed using Rogers RO3003 (with dielectric constant 3 and loss tangent 0.001) as substrate material having a thickness of 60 mils. The width W_f and gap g (between feed line and ground plane) of CPW feed line are calculated through typical design equations [1]. As shown in Fig. 5, the antenna is composed of an I-shaped radiating patch, a grounded spiral slot, a rectangular stub in lower left corner, and a pair of asymmetric inverted-L grounded strips in upper and lower right corners. The overall dimension of the proposed antenna is $20 \times 20 \text{ mm}^2$. Extensive simulation is carried out to optimize the design parameters of current research work using CST MWS and HFSS. The optimized dimensions are listed in Table 1.

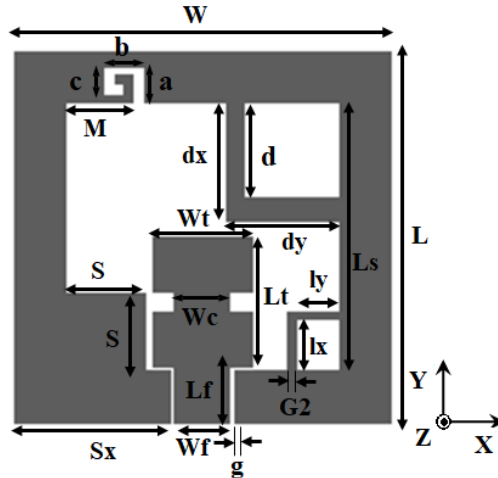


Figure 5. Design layout of proposed CPW-fed printed square slot antenna.

Table 1. Optimized dimensions of proposed CPW-fed printed square slot antenna.

Parameter	L	W	L_f	W_f	W_n	W_c	g	S_x	a	b	c
Value (mm)	20	20	3.2	3	5.2	3	0.3	8.2	2	2	1.5
Parameter	L_t	S	L_s	h	M	d	dx	dy	l_x	l_y	G_2
Value (mm)	6.2	4.2	14.4	1.524	3	5	6.4	6	2.20	2.70	0.5

3.2. Design Procedure

In this section, design procedure of the antenna is described by using four design stages. Fig. 6 depicts the realization for current research work with the help of four antenna stages. The magnitude of reflection coefficient and axial ratio (AR) curves for Ant. 1 to Ant. 4 are shown in Figs. 7(a) and (b), respectively. In the first stage, a CPW-fed I-shaped radiating patch square slot antenna [named as Ant. 1] is designed as shown in Fig. 6. It gives linear polarization ($AR > 40$ dB) and wide IBW as depicted in Fig. 7. In the second stage, a rectangular stub with dimension of $S \times S$ is embedded in the lower left corner of Ant. 1 [named as Ant. 2] to enhance the IBW of antenna. It also provides additional resonance due to coupling formed between the rectangular stub and I-shaped radiating patch. In addition, it helps to generate two identical field components and quadrature phase difference (PD) which produces circular polarization capability at about 9 GHz. In the third stage, a pair of asymmetric inverted-L grounded strips is embedded in opposite corners of the CPW ground plane of Ant. 2 [named as Ant. 3] which improves ARBW of about 15% as compared to Ant. 2. Due to the coupling formed between the upper edge of I-shaped radiating patch and the lower arm of upper inverted-L grounded strip, the impedance matching is greatly improved and provides a wide impedance bandwidth. For achieving wider 3-dB ARBW within the same IBW range, a spiral slot is embedded in the top left corner of CPW ground plane of Ant. 3 [named as Ant. 4] which excites additional currents in different directions at different frequencies for the rotation of field components with equal magnitude and quadrature PD. As depicted in Fig. 6, embedding this spiral slot, the lower-edge and higher-edge frequencies of axial ratio plot are shifted and provide fine tuning towards the CP frequency band. The dimensions and position of the spiral slot dominantly affect the CP operation as depicted in Fig. 11. So the parameters of spiral slot are optimized very carefully and fixed at optimum value such that it predominantly affects CP operation of antenna, but it shows slight effect on IBW [19, 20]. It can be found that the 3-dB ARBW is greatly enhanced about 40% by embedding this spiral slot. From the evolution analysis, it can be said that the CP generated through a spiral slot, a rectangular stub, and a pair of inverted-L grounded strips provides around 60% 3-dB ARBW. Table 2 summarizes the comparative analysis of Ant. 1 to Ant. 4 in the IBW and 3-dB ARBW.

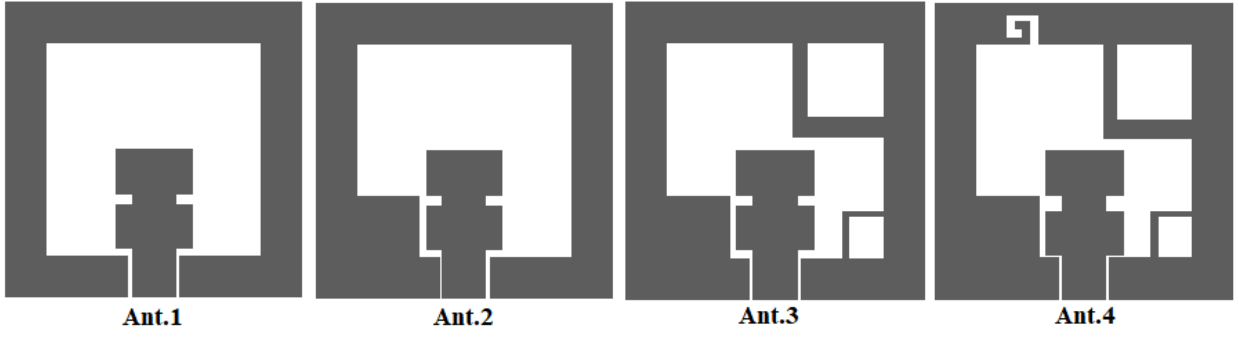


Figure 6. Antenna evolution stages to realize proposed CP antenna.

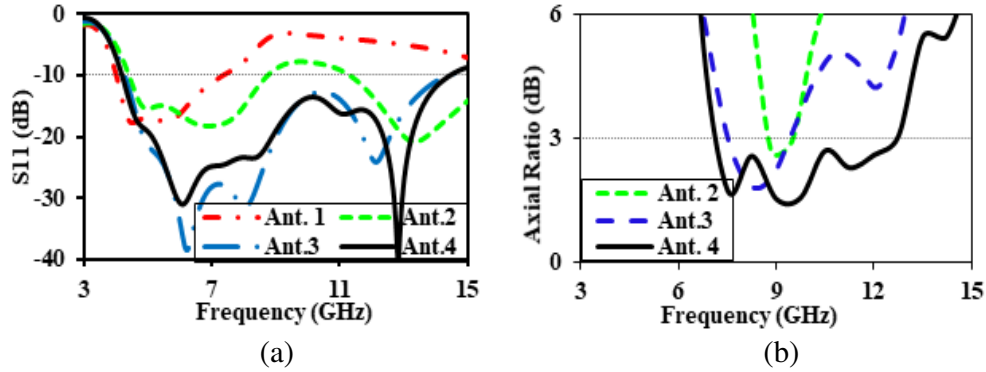


Figure 7. Simulated results for different stages (Ant. 1 to Ant. 4) (a) $|S_{11}|$ and (b) axial ratio.

Table 2. Comparative analysis for Ant. 1 to Ant. 4.

Antenna Configuration	IBW (GHz, f_c , %)	3-dB ARBW (GHz, f_c , %)	Antenna response
Ant. 1	4.0–7.1; 5.55; 55.85	-	Single-band
Ant. 2	4.4–8.7; 6.55; 65.64 11.32–16; 13.66; 34.26	8.8–9.5; 9.15; 7.65	Dual-band
Ant. 3	4.1–14.1; 9.1; 109.90	7.5–9.44; 8.47; 22.90	Single-band
Ant. 4 (Proposed antenna)	4.1–14.54; 9.32; 112	6.47–12; 9.23; 60	Single-band

3.3. Analysis of Circular Polarization Mechanism

In order to analyze the CP mechanism of the proposed antenna, the surface current distributions at two frequencies 8 GHz and 10.5 GHz with varying phases are depicted in Figs. 8(a) and (b), respectively. From Fig. 8(a), it can be noted that the maximum currents on the rectangular stub, upper side radiating element, upper inverted-L grounded strip, and vertical CPW ground arm of gap between inverted-L grounded strips are oppositely directed at $\omega t = 0^\circ$.

Similarly, from Fig. 8(b), it can be noted that the maximum currents on spiral slot, lower inverted-L grounded strip, and upper side radiating element are oppositely directed at $\omega t = 0^\circ$. So, the addition of current vectors on these elements can generate dominant current vector in both cases. Therefore, the resultant current vector rotated at both frequencies from $\omega t = 0^\circ$ to 270° in clockwise direction which gives left hand circular polarization (LHCP) in the broadside direction.

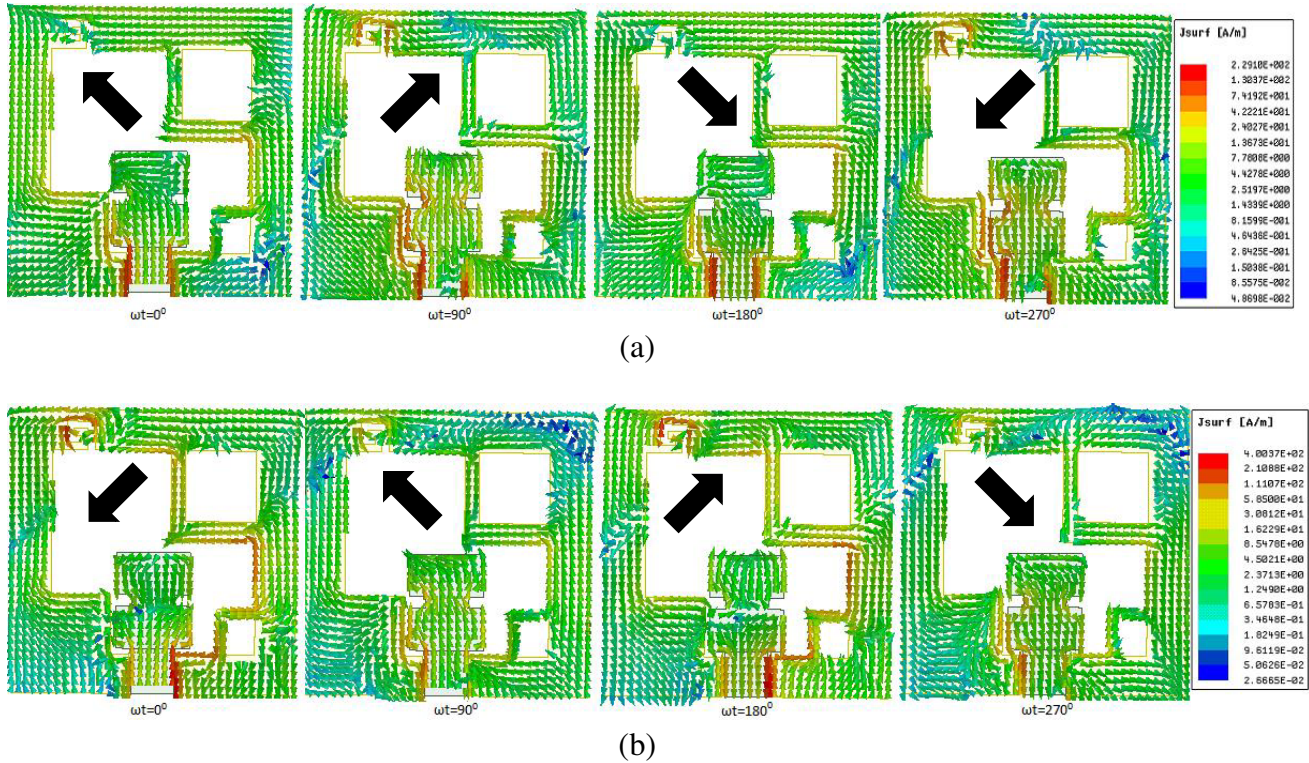


Figure 8. Surface current distribution over the proposed antenna at (a) 8 GHz and (b) 10.5 GHz.

3.4. Parametric Analysis

This segment is explained in order to investigate the response of the IBW and 3-dB ARBW employing some key parameters throughout the parametric realization. The key parameters of the proposed antenna are S (dimension of rectangular stub), W_n (width of I-shaped radiating element), and M (position of spiral slot) considered to optimize values by using EM simulator.

3.4.1. Effect of Variation in S (Dimension of Rectangular Stub)

Due to variation in the dimension of grounded rectangular stub, the IBW and 3-dB ARBW are greatly affected as observed from Fig. 9. It can be observed that the value of S is increased from 1 mm to

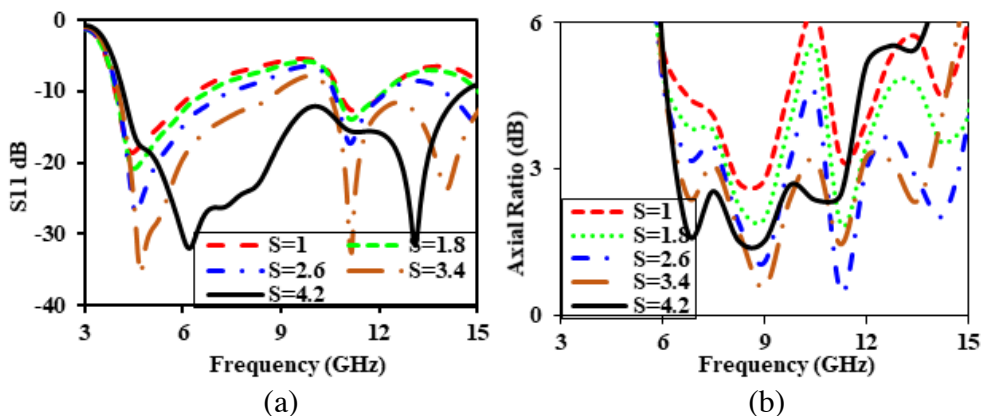


Figure 9. Effect of variation in S (dimension of rectangular stub) (a) $|S_{11}|$ and (b) AR.

4.2 mm, with step size 0.8 mm, and the value of IBW changes from dual/multi-band to wideband as shown in Fig. 9(a). Fig. 9(b) illustrates that increasing the value of S , 3-dB ARBW is enhanced due to perturbation of the current mainly on the rectangular stub. Meanwhile, the rectangular stub could be considered as a coupled element with the radiating patch. Therefore, by properly optimizing its dimensions, the desired IBW and 3-dB ARBW can be achieved to maintain the coupling between elements. Finally, S is chosen as 4.2 mm for getting the widest 3-dB ARBW and IBW.

3.4.2. Effect of Variation in W_n (Width of Radiating Patch)

The effects of variation in width of radiating element on IBW and 3-dB ARBW are shown in Figs. 10(a) and (b), respectively. Varying W_n from 3 mm to 5.2 mm affects the IBW and AR bandwidth. Fig. 10(a) illustrates that with the increased value of W_n , the impedance matching is improved due to maintaining the coupling among nearby elements and provides wide impedance bandwidth. Similarly, Fig. 10(b) illustrates that the increased value of W_n parameter mainly has impact on upper edge-frequency which enhances the 3-dB ARBW due to the perturbation of current on the radiating patch. So, we select the optimal value of $W_n = 5.2$ mm to get the widest IBW and 3-dB ARBW.

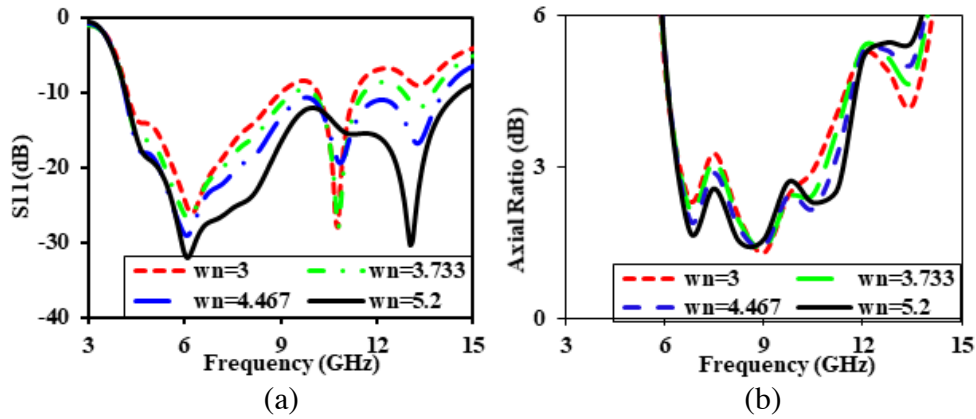


Figure 10. Effect of variation in W_n (width of radiating patch) (a) $|S_{11}|$ and (b) AR.

3.4.3. Effect of Variation in M (Position of Spiral Slot)

Due to variation in the position of the spiral slot, the IBW is slightly affected while it has a great impact on AR bandwidth of the proposed antenna as observed from Fig. 11. By increasing the position M of

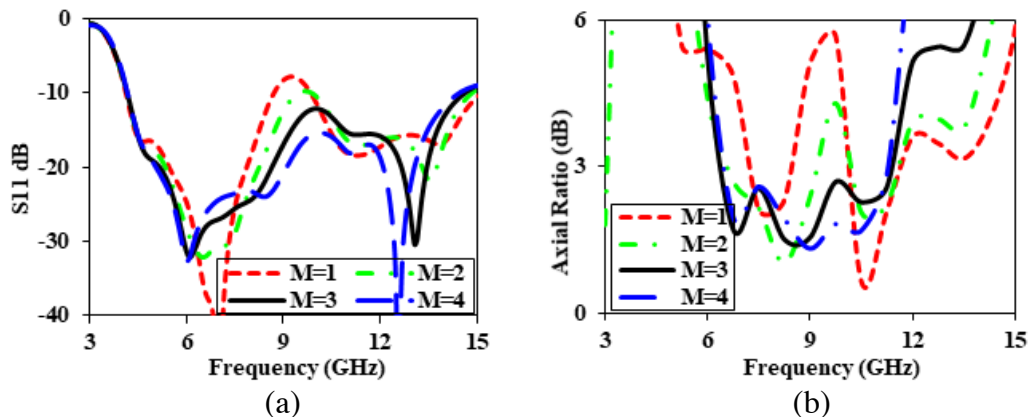


Figure 11. Effect of variation in M (position of spiral slot) (a) $|S_{11}|$ and (b) AR.

spiral slot from 1 mm to 4 mm, the upper edge frequency of IBW is decreased with a small percentage as shown in Fig. 11(a). However, AR bandwidth is greatly increased as shown in Fig. 11(b) due to perturbation of the current on the spiral slot. By properly choosing the value of M , the desired IBW and 3-dB ARBW can be achieved. So, we select $M = 3$ mm for getting the widest ARBW.

4. EXPERIMENTAL RESULTS AND DISCUSSION

A prototype of the strips and spiral slot loaded circularly polarized PSSA has been fabricated on an RO3003 substrate (as shown in Fig. 12) as per optimized dimensions listed in Table 1. The measured results to verify the simulated (using CST MWS and HFSS v.16.0) results are presented. The magnitude of S -parameters is measured using R&S ZNB vector network analyzer (VNA), and radiation characteristics are measured using an anechoic chamber.

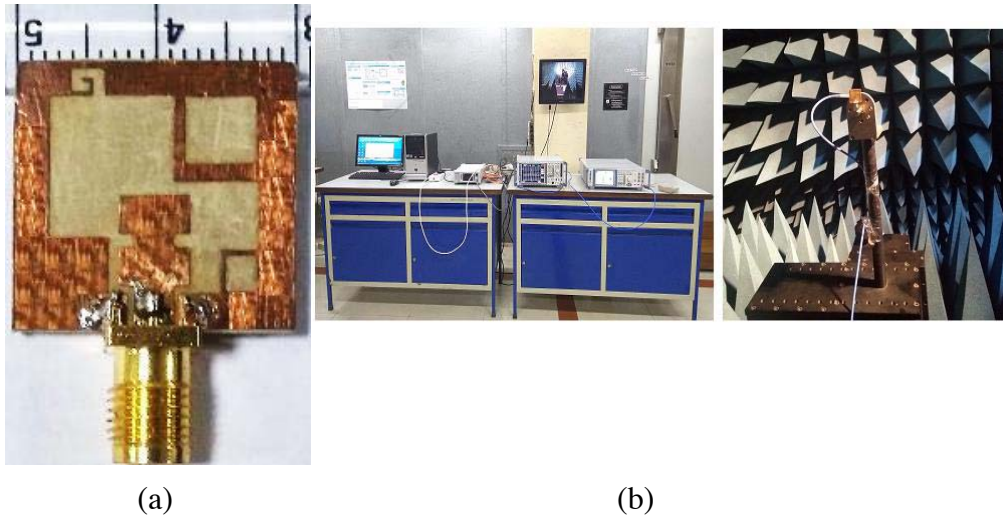


Figure 12. (a) Photograph of fabricated spiral slot loaded CPSSA antenna and (b) its measurement setup.

4.1. S -Parameter and Axial Ratio

The simulated (using CST MWS and HFSS) and measured $|S_{11}|$ and AR plot are depicted in Fig. 13, where good agreement between them is obtained. From Fig. 13(a), the measured IBW is 115.78% (4–15 GHz), and the simulated bandwidth is 112% (4.1–14.54 GHz) using CST MWS and 104% (4.39–14.04 GHz) using HFSS software. The anechoic chamber setup is used to measure the AR in broadside direction (i.e., $\theta = 0^\circ$, and $\phi = 0^\circ$ angles). The measured 3-dB ARBW is 56.52% (6.6–11.8 GHz), and simulated 3-dB ARBW is 60% (6.47–12 GHz) using CST MWS and 54.87% (6.89–12.1 GHz) using HFSS software. The summary of the simulated and measured $|S_{11}|$ and AR are listed in Table 3.

Table 3. Comparison of simulated and measured $|S_{11}|$ and AR results.

Methods	Impedance Bandwidth		3-dB ARBW	
	GHz	%	GHz	%
CST MWS	4.1–14.54	112	6.47–12	60
HFSS	4.39–14.04	104	6.89–12.1	54.87
Measured	4–15	115.78	6.6–11.8	56.52

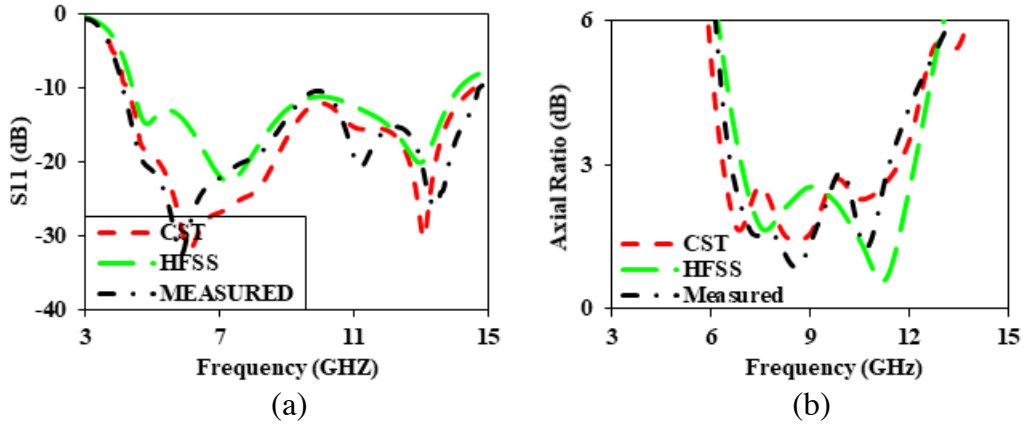


Figure 13. Simulated and measured (a) $|S_{11}|$ and (b) axial ratio.

4.2. Input Impedance and Gain Measurement

Figure 14(a) shows that the proposed strips and spiral slot loaded printed square slot antenna. The real part (resistance) approaches 50Ω , and imaginary part (reactance) reaches near zero as obtained through CST MWS and HFSS software. Fig. 14(b) shows the simulated and measured peak gains of the proposed antenna. The measured peak gain value is 5.5 dBi, simulated peak gain value is 5.38 dBi using CST MWS and 6.3 dBi using HFSS software. The gain value near 11 GHz is slightly decreased due to impedance mismatching as observed in input impedance curve.

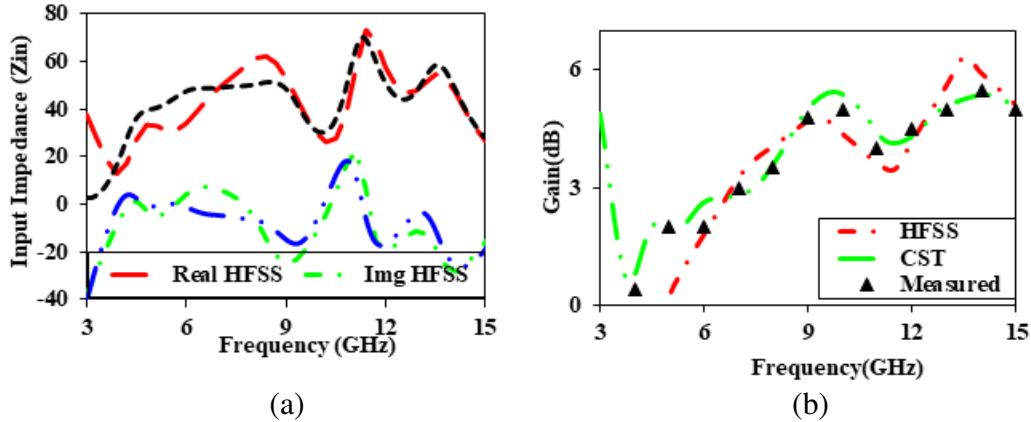


Figure 14. (a) Simulated input impedance plot and (b) measured and simulated gain plot.

4.3. Radiation Pattern Measurement

The simulated and measured radiation patterns of the proposed antenna at 8 GHz and 10.5 GHz frequencies in xz -plane ($\phi = 0^\circ$) and yz -plane ($\phi = 90^\circ$) areas are shown in Figs. 15(a) and (b), respectively, where good agreement between them is observed. From the bidirectional property of the proposed CP antenna, it is observed that the antenna radiates LHCP wave in upper hemisphere (i.e., $+Z$ direction) and right hand CP (RHCP) wave in lower hemisphere (i.e., $-Z$ direction). Also, a good cross polarization level (at $\theta = 0^\circ$) is achieved in the LHCP and RHCP radiation patterns which show good circular polarization radiation. At 10.5 GHz frequency, the radiation pattern in yz -plane is slightly deviated from the main axis (i.e., $\theta = 0^\circ$) because of rectangular stub added in lower left corner of CPW ground plane. Table 4 shows the ranges of angles in broadside direction at CP frequencies where $AR \leq 3$ dB is observed.

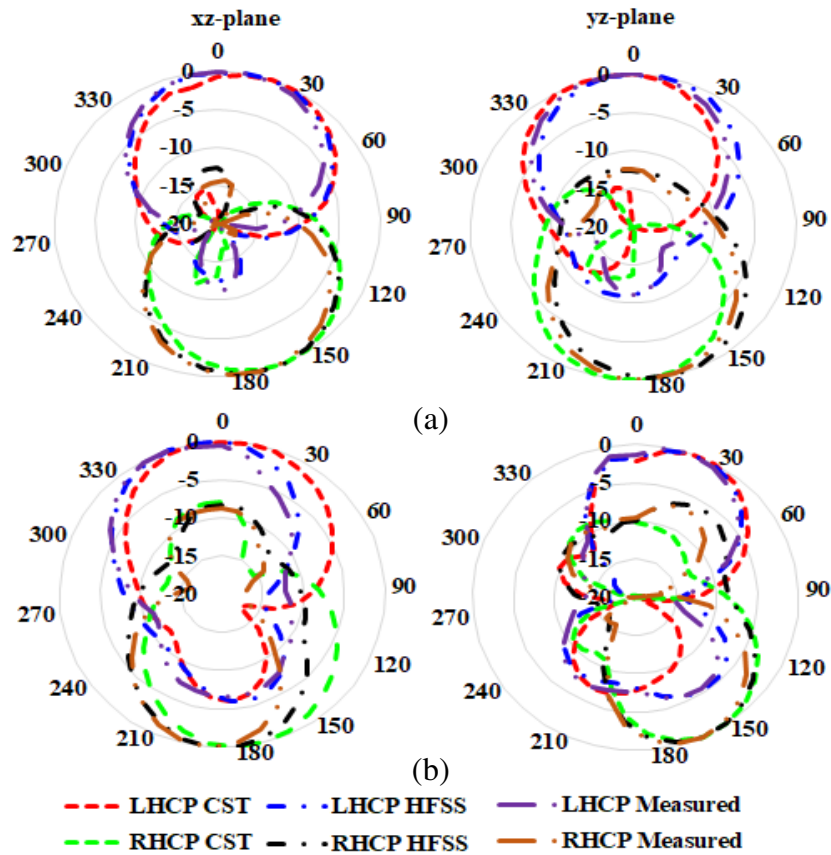


Figure 15. Radiation pattern of the proposed antenna at (a) 8 GHz and (b) 10.5 GHz.

Table 4. Range of angles (θ and ϕ), where the AR \leq 3 dB in broadside direction of radiation pattern.

Frequency (GHz)	8	10.5
Polarization	LHCP	LHCP
$\phi = 0^\circ$	$\theta = 5^\circ$	$\theta = 0^\circ$
$\phi = 90^\circ$	$\theta = 0^\circ$	$\theta = 15^\circ$

Table 5 summarizes the 3-dB beamwidths of proposed antenna at 8 GHz and 10.5 GHz in xz -plane and yz -plane. It provides wide 3-dB beamwidth at both frequencies. It is also observed that beamwidth decreases as gain increases (more directive) with frequency, which satisfies the basic antenna theory concept [1].

Table 6 shows the comparison of proposed antenna with reported literature on broadband CP antennas. Reported antennas in [4–7], provide wideband/multiband CP response with small 3-dB ARBW and IBW and relatively large size. The antennas reported in [8–18] provide broadband CP with large physical dimensions, narrow 3-dB ARBW bandwidth, and small gain as compared to the proposed antenna. The proposed broadband CP antenna has 56.67% 3-dB ARBW and 5.5 dBi gain which are better than the cited antennas in the literature as compared in Table 6. Moreover, it can be concluded that this antenna geometry provides small size, simply structured geometry, widest 3-dB ARBW, and high gain about 5.5 dBi.

Table 5. 3-dB beam width of proposed antenna.

Simulation Software	Plane	RHCP	LHCP	RHCP	LHCP
		at 8 GHz		at 10.5 GHz	
CST MWS	$\phi = 0^\circ$ (xz -plane)	79.8	78.3	81.5	82.2
	$\phi = 90^\circ$ (yz -plane)	79.1	76.2	62.2	58.8
HFSS	$\phi = 0^\circ$ (xz -plane)	83	82	70.1	70.12
	$\phi = 90^\circ$ (yz -plane)	80.5	79	62.3	57.3

Table 6. Comparison table of proposed antenna with reported literature.

Ref.	Antenna size (mm ²)	IBW (GHz, f_c , %)	3-dB ARBW (GHz, f_{cp} , %)	Measured Peak gain (dBi)	CP response
[4]	25 × 25 × 1	3.15–7.75, 5.45, 84.4	5.12–7.15, 6.14, 33	3.37	Wideband
[5]	28 × 28 × 1.6	3.25–8, 5.63, 84.4	4.4–6.67, 5.34, 41.3	3	Wideband
[6]	40 × 40 × 1.6	2.3–3.45, 2.87, 40 3.85–4.65, 4.25, 18.8	2.9–3.65, 3.2, 23.43	3–4	wideband
[7]	40 × 46 × 1.6	2.02–3.10, 2.7, 40 4.57–6.88, 5.8, 39.8	2.6–3.2, 2.9, 22.2 4.85–6.0, 5.43, 19.8	1.8 5.5	Dual band
[8]	44.7 × 53 × 1.6	2.49–6.42, 4.46, 88.2	2.72–4.49, 3.6, 50	3.5	Broadband
[9]	50 × 50 × 0.8	2.13–7.46, 4.8, 111	3.2–4.2, 3.7, 27	5.3	Broadband
[10]	60 × 60 × 0.8	2.67–13, 7.84, 132	4.9–6.9, 5.9, 32.2	4.2	Broadband
[11]	60 × 60 × 0.8	2.023–3.421, 2.72, 51.4	2.07–3.41, 2.75, 48.8	3.4	Broadband
[12]	40 × 40 × 1.6	5.02–10.84, 7.93, 73.39	5.07–9.22, 7.15, 58.08	4.22	Broadband
[13]	21.5 × 21.5 × 1.6	8.4–15.2, 11.8, 57.33	9.7–3, 11.41, 28.64	4.8	Broadband
[14]	32 × 30 × 1.6	3.92–7.52, 5.74, 62.94	4.28–7.44, 5.86, 53.92	-	Broadband
[15]	30 × 30 × 1.6	3.32–6.9, 6.48, 70.1	4.5–6.55, 5.5, 37.1	4.1	Broadband
[16]	39 × 32 × 1.6	2.4–7.4, 4.9, 102.04	4.9–6.9, 5.9, 37.5	2.4	Broadband
[17]	20 × 20 × 0.8	2.95–14, 8.48, 130	3.72–7.10, 5.42, 35.7	4.2	Broadband
[18]	63 × 58 × 1.5	1.5–3.3, 2.4, 72	1.98–3.3, 2.5, 41.6	2.4	Broadband
Prop. work	20 × 20 × 1.5	4.0–15, 9.5, 115.78	6.6–11.82, 9.21, 56.67	5.5	Broadband

5. CONCLUSION

In this work, a compact CPW-fed broadband circularly polarized PSSA with wide ARBW based on CMA has been designed and analyzed for C-band and X-band applications. CMA provides the guidance for finding the dominant modes, feedline position, and responsible parameters for radiations. A prototype of the optimized structure has been fabricated and tested which gives the measured ARBW and IBW of the proposed antenna, 56.67% (6.6–11.8 GHz) and 115.78% (4–15 GHz), respectively. The broadband CP performance of the proposed antenna over a large IBW, simply structured, compact in size, LHCP radiations over wide angle range, and high gain makes it an excellent candidate for wireless and satellite application especially in C-band and X-band applications.

ACKNOWLEDGMENT

The authors would like to acknowledge and convey their sincere thanks to the Department of Electronics and Communication Engineering, Banasthali Vidyapith, Niwai, Tonk, India and Department of Electronics and Communication Engineering, G.B. Pant Govt. Engineering College, New Delhi, India for providing necessary facilities of measurement to complete this research work.

REFERENCES

1. Gao, S. S., Q. Luo, and F. Zhu, *Circularly Polarized Antennas*, Wiley-IEEE Press, UK, 2013.
2. Lin, Y. F., H. M. Chen, and S. C. Lin, "A new coupling mechanism for circularly polarized annular-ring patch antenna," *IEEE Trans. Antennas Propag.*, Vol. 56, 11–16, Jan. 2008.
3. Prajapati, P. R., G. G. K. Murthy, A. Patnaik, and M. V. Kartikeyan, "Design and testing of a compact circularly polarised microstrip antenna with fractal defected ground structure for L-band applications," *IET Microw. Antennas Propag.*, Vol. 9, No. 11, 1179–1185, 2015.
4. Kumar, A., J. K. Deegwal, and M. M. Sharma, "Miniaturized wideband dual linearly and circularly polarized printed square slot antenna for multiradio wireless systems," *Int. J. Electron Commun.*, Vol. 88, 44–51, 2018.
5. Nosrati, M. and N. Tavassolian, "Miniaturized circularly polarized square slot antenna with enhanced axial-ratio bandwidth using an antipodal Y-strip," *IEEE Antennas Wireless Propag. Lett.*, Vol. 16, 817–820, 2016.
6. Pirooj, A., M. Naser-Moghadasi, F. B. Zarrabi, and A. Sharifi, "A dual band slot antenna for wireless applications with circular polarization," *Progress In Electromagnetics Research C*, Vol. 71, 69–77, 2017.
7. Xin, Y., Q. Feng, and J. Tao, "A CPW-fed dual-band slot antenna with circular polarization," *Progress In Electromagnetics Research Letters*, Vol. 61, 77–83, 2016.
8. Guo, J.-L., J.-N. Zhou, Y.-B. Guan, and B.-H. Sun, "A broadband circularly polarized slot antenna with a compact microstrip to CPW transition," *Int. J. RF Microw. Comput. Aided Eng.*, Vol. 28, No. 5, e21260, 2018.
9. Jan, J.-Y., C.-Y. Pan, K.-Y. Chiu, and H.-M. Chen, "Broadband CPW-fed circularly-polarized slot antenna with an open slot," *IEEE Trans. Antennas Propag.*, Vol. 61, No. 3, 1418–1422, 2013.
10. Pourahmadazar, J., C. Ghobadi, J. Nourinia, N. Felegari, and H. Shirzad, "Broadband CPW-fed circularly polarized square slot antenna with inverted-L strips for UWB applications," *IEEE Antennas Wireless Propag. Lett.*, Vol. 10, 369–372, 2011.
11. Sze, J.-Y., C.-G. Hsu, Z.-W. Chen, and C.-C. Chang, "Broadband CPW-fed circularly polarized square slot antenna with lightning-shaped feedline and inverted-L grounded strips," *IEEE Trans. Antennas Propag.*, Vol. 58, No. 3, 973–977, 2010.
12. Midya, M., S. Bhattacharjee, and M. Mitra, "Pair of grounded L strips loaded broadband circularly polarised square slot antenna with enhanced axial ratio bandwidth," *Electron. Lett.*, Vol. 54, No. 15, 917–918, 2018.
13. Verma, M. K., B. K. Kanaujia, J. P. Saini, and P. Saini, "A novel circularly polarized gap-coupled wideband antenna with DGS for X/Ku-band applications," *Electromagnetics*, Vol. 39, No. 3, 186–197, 2019.
14. Midya, M., S. Bhattacharjee, and M. Mitra, "Broadband circularly polarized planar monopole antenna with G-shaped parasitic strip," *IEEE Antennas Wireless Propag. Lett.*, Vol. 18, No. 4, 581–585, Apr. 2019.
15. Oteng Gyasi, K., J. Li, Y. Huang, and W. Guangjun, "Broadband circularly polarized square slot antenna with a G-shaped feedline," *Microw. Opt. Technol. Lett.*, Vol. 59, 3055–3063, 2017.
16. Jhajharia, T., V. Tiwari, D. Yadav, S. Rawat, and D. Bhatnagar, "Wideband circularly polarised antenna with an asymmetric meandered-shaped monopole and defected ground structure for wireless communication," *IET Microw. Antennas Propag.*, Vol. 12, No. 9, 1554–1558, Jul. 2018.

17. Karamzadeh, S., V. Rafii, M. Kartal, and H. Saygin, "Compact UWB CP square slot antenna with two corners connected by a strip line," *Electron. Lett.*, Vol. 52, No. 1, 10–12, 2016.
18. Han, R. and S. Zhong, "Broadband circularly-polarised chifre-shaped monopole antenna with asymmetric feed," *Electron. Lett.*, Vol. 52, No. 4, 256–258, 2016.
19. Chen, C. and E. K. N. Yung, "Dual-band dual-sense circularly-polarized CPW-fed slot antenna with two spiral slots loaded," *IEEE Trans. Antennas Propag.*, Vol. 57, No. 6, 1829–1833, 2009.
20. Sadeghi, P., J. Nourinia, and C. Ghobadi, "Square slot antenna with two spiral slots loaded for broadband circular polarisation," *Electron. Lett.*, Vol. 52, No. 10, 787–788, May 12, 2016.
21. Garbacz, R. J., "Modal expansions for resonance scattering phenomena," *Proc. IEEE*, Vol. 53, No. 8, 856–864, 1965.
22. Harrington, R. F. and J. R. Mautz, "The theory of characteristic modes for conducting bodies," *IEEE Trans. Antennas Propag.*, Vol. 19, No. 5, 622–628, 1971.
23. Lau, B. K., D. Manteuffel, H. Arai, and S. V. Hum, "Guest editorial theory and applications of characteristic modes," *IEEE Trans. Antennas Propag.*, Vol. 64, No. 7, 2590–2594, Jul. 2016.
24. Yang, X., Y. Liu, and S.-X. Gong, "Design of a wideband omnidirectional antenna with characteristic mode analysis," *IEEE Antennas Wireless Propag. Lett.*, Vol. 17, No. 6, 993–997, 2018.
25. Zhao, X., S. P. Yeo, and L. C. Ong, "Planar UWB MIMO antenna with pattern diversity and isolation improvement for mobile platform based on the theory of characteristic modes," *IEEE Trans. Antennas Propag.*, Vol. 66, No. 1, 420–425, 2018.
26. Zhang, Q. and Y. Gao, "Compact low-profile UWB antenna with characteristic mode analysis for UHF TV white space devices," *IET Microw. Antennas Propag.*, Vol. 11, No. 11, 1629–1635, 2017.
27. Wu, W. and Y. P. Zhang, "Analysis of ultra-wideband printed planar quasi-monopole antennas using the theory of characteristic modes," *IEEE Trans. Antennas Propag. Mag.*, Vol. 52, No. 6, 67–77, 2010.
28. Tran, H. H., N. Nguyen-Tron, and A. M. Abbosh, "Simple design procedure of a broadband circularly polarized slot monopole antenna assisted by characteristic mode analysis," *IEEE Access*, Vol. 6, 78386–78396, 2018.
29. Ghalib, A. and M. S. Sharawi, "New antenna mode generation based on theory of characteristic modes," *Int. J. RF Microw. Comput. Aided Eng.*, e21686, 2018.
30. Lu, W.-J. and L. Zhu, "Wideband stub-loaded slotline antennas under multi-mode resonance operation," *IEEE Trans. Antennas Propag.*, Vol. 63, No. 2, 818–823, 2015.
31. Garbacz, R. J. and R. H. Turpin, "A generalized expansion for radiated and scattered fields," *IEEE Trans. Antennas Propag.*, Vol. 19, No. 3, 348–358, Mar. 1971.